Catalysis Today xxx (2015) xxx–xxx

Contents lists available at ScienceDirect

Catalysis Today

journal homepage: www.elsevier.com/locate/cattod

Palladium nanoparticles supported on CNT functionalized by rare-earth oxides for solvent-free aerobic oxidation of benzyl alcohol

Yibo Yan, Xinli Jia, Yanhui Yang*

School of Chemical and Biomedical Engineering, Nanyang Technological University, Singapore 637459, Singapore

ARTICLE INFO

Article history:
Received 18 September 2014
Received in revised form 22 July 2015
Accepted 24 July 2015
Available online xxx

Keywords:
Rare-earth oxides
CNT surface functionalization
Supported Pd catalyst
Electrochemical measurement
Aerobic oxidation of benzyl alcohol

ABSTRACT

A series of rare-earth oxide functionalized multi-walled carbon nanotubes (CNTs) were prepared through wet impregnation process. Palladium nanoparticles were deposited over surfaces of functionalized CNT through metal ion adsorption–reduction method and were examined using X-ray diffraction, transmission electron microscopy, in situ adsorbed pyridine Fourier Transform Infrared spectroscopy, and electrochemical measurements. Compared to the non-functionalized Pd/CNT catalyst, the catalytic activities of different rare-earth oxide functionalized CNT supported Pd catalysts were improved for aerobic solvent-free oxidation of benzyl alcohol due to the fine-tuned properties of catalytic active sites, e.g., Pd particle size, size distribution, valence status, metal–support interactions, electron density, surface acidity and basicity. Sm_2O_3 functionalization displayed the highest improvement in catalytic activity whereas the content of Sm_2O_3 had impact on Pd particle size, electrochemical surface area, and metal–support interactions which further influenced the benzyl alcohol conversion and selectivity toward benzyl aldehyde. The catalyst functionalized by an appropriate amount of Sm_2O_3 afforded a remarkably high turnover frequency of 318,760 h^{-1} for aerobic oxidation of benzyl alcohol based upon palladium electrochemical active surface areas.

1. Introduction

Rare-earth elements have demonstrated a broad range of applications in catalysis. Rare-earth oxides-based heterogeneous catalysts have been applied in various organic chemistry reactions such as the redox, aldolization, alcohol dehydration, ketone formation, aromatic compounds alkylation, ring-open, coupling reactions and so forth due to the redox and acid–base properties [1,2]. Numerous cationic rare-earth metal complexes have been synthesized to perform as the catalysts for olefin polymerization [3,4]. Furthermore, rare-earth oxides also attracted various curiosities as a structural and electronic promoter to improve the catalyst performance over conventional supports such as silica, alumina, titania [5–10]. Well known for their lattice oxygen storage capability, rare-earth oxides have been applied into automotive catalysts [11,12], improved catalyst for soot oxidation [13], and industrial catalysts for removal of organics from waste water [14,15]. Owing to the improved basic strength and their contribution to the reducibility increase, rare-earth oxides have highly promoted the performance after their modifying Pt/SiO_2 catalysts for CO oxidation [16].

Catalyst support, such as metal oxides [17] and carbonaceous materials [18,19], play a pivotal role in the catalytic reactions. Carbon nanotubes (CNTs) are among the headlines of nanotechnology, particularly catalysis [20], due to their high purity eradicating self-poisoning, thermal stability, electrical conductivity, impressive mechanical properties, high accessibility of the active phase and absence of micro-porosity thus reducing the mass diffusion and intra-particle transfer effects in reaction medium [20–23]. As for catalysis, the metal oxide functionalities contribute to the control of the properties such as the electron conductivity, polarity, hydrophobicity and surface chemistry including amphoteric property in order to develop the CNT-based catalysts with enhanced catalytic performance for certain reactions. Zhou et al. reported that the manganese dioxide functionalized CNTs supported platinum catalysts possessed higher electrochemical active surface area and better methanol electro-oxidation activity than Pt/CNTs [24].

CNT as catalyst support has been extensively explored [25,26]. Nevertheless, reports related to rare-earth oxides as surface functionalities of CNT-supported catalysts are limited. Hence, this study is aimed to prepare rare-earth oxides LnO_x (Ln = La, Ce, Sm, Gd, Er, Yb) functionalized CNTs supported palladium catalysts considering the possible surface chemistry and electron property modification that the rare-earth oxides would bring to the catalyst.

* Corresponding author.
E-mail address: yhyang@ntu.edu.sg (Y. Yang).

http://dx.doi.org/10.1016/j.cattod.2015.07.021
0920-5861/

The obtained catalysts are evaluated through the aerobic oxidation of benzyl alcohol with molecular oxygen, which is a vitally important intermediate reaction to transform functional groups in organic synthesis and meanwhile a model aromatic alcohol oxidation reaction employed by laboratory study [27–29]. Since the first study of the Pd-catalyzed oxidation of benzyl alcohol, massive investigations have explored the role of Pd catalysts along with their applications in benzyl alcohol oxidation [30]. Surface-functionalized carbon or CNTs supported Pd catalysts [30–32] have become one of the most alluring topics after the early usage of Pd/C [33] or Pd/CNT [34] catalysts for alcohol oxidation. This investigation concerning rare earth oxides functionalized CNTs supported Pd for benzyl alcohol oxidation and the discussion on the correlation of the catalyst structure, surface chemistry, electrochemical activity and catalytic performance will be rendered in detail.

2. Experimental

2.1. Synthesis

Commercial multi-walled CNTs powder (>95%, Cnano) was purified with pretreatment in concentrated nitric acid and oxygen-containing groups were generated on CNT surfaces: slurry of CNTs powder (2 g) suspended in 100 mL of concentrated nitric acid (69%, Sigma–Aldrich) was refluxed at 120 °C for 4 h. After cooling to room temperature, vacuum filtration was performed followed by rinsing with deionized water for several times and subsequently drying at 80 °C overnight. Then the purified CNT was surface-functionalized using rare-earth nitrides $Ln(NO_3)_3{\cdot}6H_2O$ (Ln = La, Ce, Sm, Gd, Er, Yb) prior to adsorbing palladium precursors. 0.25 g of pretreated CNTs powder and a certain amount of rare-earth nitride $Ln(NO_3)_3{\cdot}6H_2O$ were suspended in 20 mL of deionized water, where the content of rare-earth element was controlled at 5 wt.%. After stirring for 4 h and aging for 12 h, the mixture was evaporated at 80 °C in a water bath and dried at 80 °C overnight, followed by calcination in tube furnace at 400 °C for 4 h under nitrogen flow to afford LnO_x/CNT composites. Adsorption–reduction method reported by Chi et al. [35] was employed to deposit palladium nanoparticles onto LnO_x/CNT functionalized support. 379.7 μL of 0.05 M $PdCl_2$ aqueous solution was added to 0.2 g of LnO_x/CNT suspended in 20 mL of deionized water, followed by refluxing at 80 °C for 5 h. The suspension was filtered, washed and dried overnight. After reduction in hydrogen flow at 400 °C for 2 h, the catalysts, denoted as Pd/LnO_x-CNT (Ln = La, Ce, Sm, Gd, Er, Yb), were obtained.

2.2. Characterizations

Powder X-ray diffraction (XRD) was conducted on a Bruker AXS D8 X-ray diffractometer, using filtered Cu-Kα radiation (λ = 0.15406 nm), under ambient conditions; operation condition was 40 kV and 40 mA. Data collections were between 10 and 80° (2θ) with the step length of 0.02° (2θ) per second. Inductively coupled plasma (Dual-view Optima 5300 DV ICP-OES system) was attempted to measure the metallic element contents of each catalyst using concentrated nitric acid (>69%) to dissolve the samples prior to the measurements. Transmission electron microscope (TEM) was conducted on a JEOL 2010, operating at 200 kV. Samples suspended in ethanol were dropped onto holey carbon-coated Cu grids. X-ray photoelectron spectroscopy (XPS) characterization was conducted on VG Escalab 250 spectrometer with aluminum Kα 1846.6 eV anode. The 1*s* peak of carbon at 284.6 eV was employed as the standard reference for calibration of binding energy.

In situ pyridine adsorbed Fourier Infrared spectra were recorded on a PerkinElmer Spectrum One FTIR spectrometer with potassium bromide (KBr) pellets (4000–450 cm^{-1}, resolution of 1 cm^{-1}). Samples were pressed with KBr into pellets and placed into an in situ IR cell. Prior to measurements, each sample was dehydrated at 250 °C for 1 h afterward introducing pyridine vapor flow at 50 °C till saturation. In situ IR cell was purged by helium for 30 min at a series of step-like temperatures, 50, 100, 150, and 200 °C. Spectra were recorded at room temperature after strip of background.

Cyclic voltammetry (CV) and CO stripping voltammetry were performed in a 1.0 M KOH solution at 50 mV s^{-1} using the Versa STAT 3 Potentiostat/Galvanostat (Princeton Applied Research). Catalyst ink was prepared by ultrasonically suspending 2 mg of catalyst into 3 mL of 0.025 wt.% Nafion in ethanol solution. The working electrode was prepared through dropping 30 μL of ink onto a glassy carbon electrode. Hg/HgO (1.0 M KOH) electrodes and Pt foil were respectively employed as reference and counter electrodes. Potentials of CV test were controlled in a range between −0.8 and 0.3 V. CO stripping was carried out in this way: after purging nitrogen into electrolyte for 20 min, CO was purged for 15 min to form CO layer on the catalyst surfaces while the potential was maintained at −0.8 V. Surplus CO was expelled by nitrogen bubbles. Potentials of CO stripping were also ranged between −0.8 and 0.3 V.

2.3. Aerobic oxidation of benzyl alcohol

The catalytic reaction was carried out using molecular oxygen under solvent-free conditions. Benzyl alcohol (5.174 mL, 50 mmol) was loaded in a glass flask pre-charged with 0.01 g of catalyst. The mixture was immersed in a 160 °C of oil bath while gaseous oxygen was purged (20 mL min^{-1}) to initiate the reaction. The reaction was allowed to go on for 1 h under vigorous stirring (1200 rpm). After the reaction, the solid catalyst was filtered off while the liquid phase was analyzed by Agilent gas chromatograph 6890 equipped with HP-5 capillary column. Dodecane was used as the internal standard to measure the percentage of remaining reactant and products so as to calculate benzyl alcohol conversion and benzaldehyde selectivity values [36]. The conversion, selectivity, turnover frequency (TOF) as well as the quasi-turnover frequency (qTOF) is defined as follows [37,38].

$$\text{Conversion}\ (\%) = \frac{\text{moles of reactant converted}}{\text{moles of reactant in feed}} \times 100\%$$

$$\text{Selectivity}\ (\%) = \frac{\text{moles of product formed}}{\text{moles of reactant converted}} \times 100\%$$

$$\text{TOF}\ (h^{-1}) = \frac{\text{moles of reactant converted}}{\text{moles of Pd} \times \text{reaction time}\ (h)}$$

$$\text{qTOF}\ (h^{-1}) = \frac{\text{moles of reactant converted}}{\text{moles of Pd} \times \text{dispersion} \times \text{reaction time}\ (h)}$$

$$\text{dispersion} = \frac{\text{electroactive surface area}}{(1/\text{atomic weight of Pd}) \times (N_A \times 4\pi R_{Pd}^2)}$$

3. Results and discussion

3.1. Effect of rare-earth oxides functionalities

Fig. 1 displays the XRD patterns of Pd/LnO_x-CNT catalysts with different rare-earth oxides. The diffraction peaks at 26.01° and 42.80° are respectively ascribed to the (0 0 2) and (1 0 0) facets of graphitic CNT [32]. The diffraction peaks at 40.00°, 46.07°, 68.30° shown in each catalyst are in correspondence with the (1 1 1), (2 0 0), and (2 2 0) facets respectively of palladium face-centered cubic (FCC) structure. According to Bragg's law [39], the lattice *d*-spacing of (1 1 1) plane calculated is approximately 0.225 nm which is further verified by HRTEM shown in Fig. 2. Thus, rare-earth oxides surface functionalities did not result in lattice contraction within Pd

Please cite this article in press as: Y. Yan, et al., Palladium nanoparticles supported on CNT functionalized by rare-earth oxides for solvent-free aerobic oxidation of benzyl alcohol, Catal. Today (2015), http://dx.doi.org/10.1016/j.cattod.2015.07.021

crystal lattice. The approximate full width at half max (FWHM) of (1 1 1) diffraction peak at 40.00° is in agreement with the Pd particles average size of 8 nm for 1Pd/CNT catalyst according to the Scherrer equation [40,41]. Similarly, the FWHM of 1.14° at 40.00° is indexed to the average Pd size around 7 nm for 1Pd/5Er-CNT and 1Pd/5Yb-CNT catalysts. The FWHM of 1.24° at 40.00° corresponds to the Pd particle average size around 6 nm for 1Pd/5Gd-CNT, and 1Pd/5La-CNT catalysts. The FWHM of 1.43° at 40.00° indicates the Pd grain average size of about 4 nm in Pd/5Sm-CNT and 1Pd/5Ce-CNT catalysts. The rare-earth oxides functionalities can improve the hydrophilicity of CNT surfaces, and then can increase the affinity to the aqueous palladium chloride. Therefore, the deposition of Pd precursor and the formation of small Pd particles are favored. Moreover, the positively charged rare-earth cation possesses great affinity to the $[PdCl_2(OH)_2]^{2-}$ precursor, also contributing to the formation of small and highly dispersed Pd nanoparticles. This result is further corroborated by the TEM observations and Pd particle size distribution histograms shown in Fig. 2. No distinct XRD diffraction peak for rare-earth oxides can be detected, implying that the rare-earth oxides have been homogeneously dispersed over the CNT surfaces. Since the amount of rare-earth oxides are not remarkably high, grains of rare-earth oxides as well as their contact with Pd particles are hardly perceived on HRTEM images. The rare-earth cationic precursors are chemically anchored to oxygen-containing groups on CNT surfaces. Thus the rare-earth oxides are finely deposited and the grain size is well-controlled on the level of nano-dimensions.

In situ Fourier Infrared spectroscopy with pyridine adsorbed on catalyst surfaces has been widely applied to investigate the surface Lewis and Brønsted acidic sites [42–45]. As shown in Fig. 3, the pyridine molecule is retained on the surface in three modes: (1) interaction between the N electron pair and the hydrogen atom of -OH group, (2) proton transfer from surface to pyridine (Brønsted acidity) and (3) pyridine molecule coordination to electron deficient sites (Lewis acidity) [46]. Ring vibrations in the range from 1400 to 1700 cm^{-1} distinguish between pyridine adsorbed on Lewis and Brønsted acidic sites. FTIR bands centered at 1609 cm^{-1}, 1586 (or 1570, 1582, 1585, 1587) cm^{-1}, 1500 (or 1496, 1487) cm^{-1} and 1453 (or 1447, 1452, 1454, 1457) cm^{-1} have been indexed to the 8a and b, 19a and b pyridine vibrational modes attributed to electron transfer at Lewis acidic surface sites respectively. Whereas the bands at 1642 (or 1635, 1640, 1644) cm^{-1} and 1544 (or 1537, 1545, 1546, 1547) cm^{-1} are assigned to ν8a and ν8b vibrational modes of pyridine due to proton transfer (i.e., hydrogen bond) at Brønsted acidic sites [45]. The density and strength of Lewis acid site are both higher than those of Brønsted acidic site for 1Pd/CNT and 1Pd/5Ln-CNT catalysts, implying that electron deficient sites are dominant. At 50 °C, the more intense bands at 1586 cm^{-1}, 1500 cm^{-1} and 1543 cm^{-1} on 1Pd/CNT indicates that it possesses higher density of Lewis acid sites than those functionalized by rare-earth oxides nanoparticles under relatively mild conditions. This indicates that at a relatively low temperature (e.g., 50 °C), the amount of the surface oxygen-containing species (e.g., carbonyl and carboxyl) on CNT decreases after the surface-functionalization with rare-earth oxides. However, an abrupt decline of Lewis acid site density occurs on 1Pd/CNT as the temperature increases, which, on the contrary has not been observed in spectra of 1Pd/5Ln-CNT catalysts, implying that the oxygen-containing species on CNT surface are unstable at high temperatures, in agreement with the results by Guo et al. [47]. The rare-earth oxides functionalized CNT supported Pd catalysts possess higher thermal stability of surface Lewis acid sites than 1Pd/CNT catalyst. Moreover, the shifts or splits of each band demonstrate the different types of Lewis/Brønsted acidic sites that the rare-earth oxides introduce onto the CNT surface after functionalization. Among all the catalysts, the most complexity of multiple IR bands indicates the largest number of acid site types presented on Pd/5Sm-CNT with eminent thermal stability. These acidic sites can play a vital role in alcohol dehydrogenation reaction [48–52], which is commonly present in the mechanism of benzyl alcohol oxidation reaction with molecular oxygen [53].

The surface basicity is associated with their electro-chemical properties, especially the electron donor property [46]. Cyclic voltammetry measurements are carried out on 1Pd/CNT and 1Pd/5Ln-CNT catalysts and the results are shown in Fig. 4. The larger

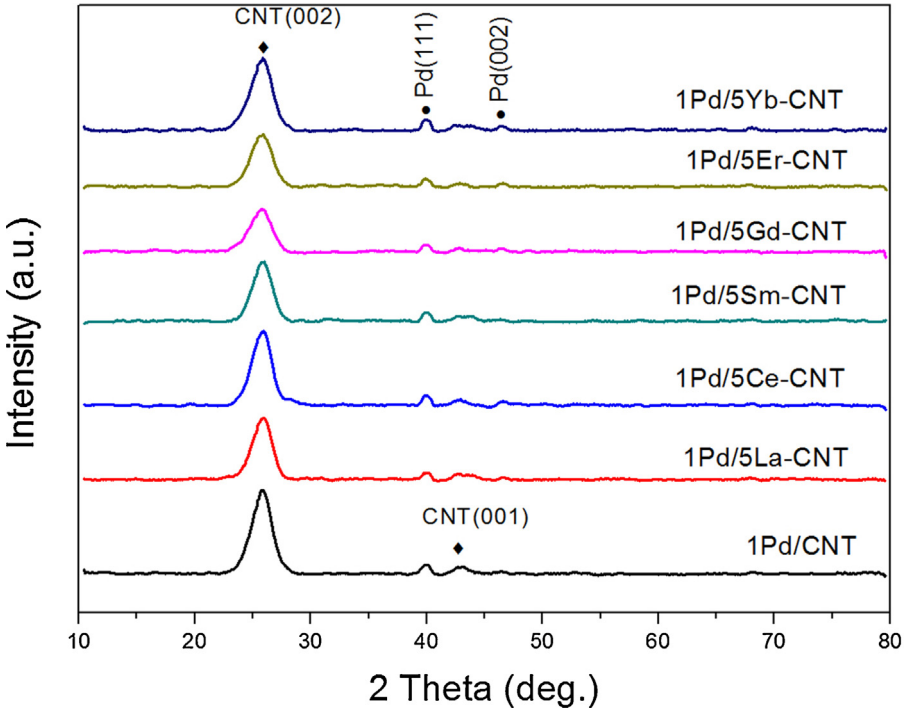

Fig. 1. XRD diffraction patterns of Pd/5Ln-CNT.

Please cite this article in press as: Y. Yan, et al., Palladium nanoparticles supported on CNT functionalized by rare-earth oxides for solvent-free aerobic oxidation of benzyl alcohol, Catal. Today (2015), http://dx.doi.org/10.1016/j.cattod.2015.07.021

area enclosed by CV background implies a higher electron density [47]. The rare-earth oxide functionalities remarkably improve the electron densities of the catalysts. As shown in Fig. 4, the background of CV signals are observed with an evident decrease in the area enclosed in the sequence of: 1Pd/5La-CNT > 1Pd/5Ce-CNT > 1Pd/5Sm-CNT ≈ 1Pd/5Gd-CNT > 1Pd/5Er-CNT > 1Pd/5Yb-CNT>1Pd/CNT. Rare-earth oxides are well known for their surface electron donor properties [54–57], which favors the enlargement of areas enclosed by CV curves, since the more redox active sites or electron donors on CNT, the larger capacitance and CV background are [58].

The sequence mentioned above is in tune with lanthanide contraction: basicity of rare-earth oxides, which is related to electron donor properties, declines with the contraction of rare-earth cation radius [59]. The absence of palladium oxide (Pd-O) reduction peak at 0.1 V for rare-earth oxides modified CNT supported Pd catalysts, except 1Pd/5Gd-CNT, indicates that Pd nanoparticles are more easily reduced to zero-valent state (Pd^0) over rare-earth oxides surface functionalized CNT supports. Surface basicity contributes to the formation of small Pd nanoparticle size and narrow size

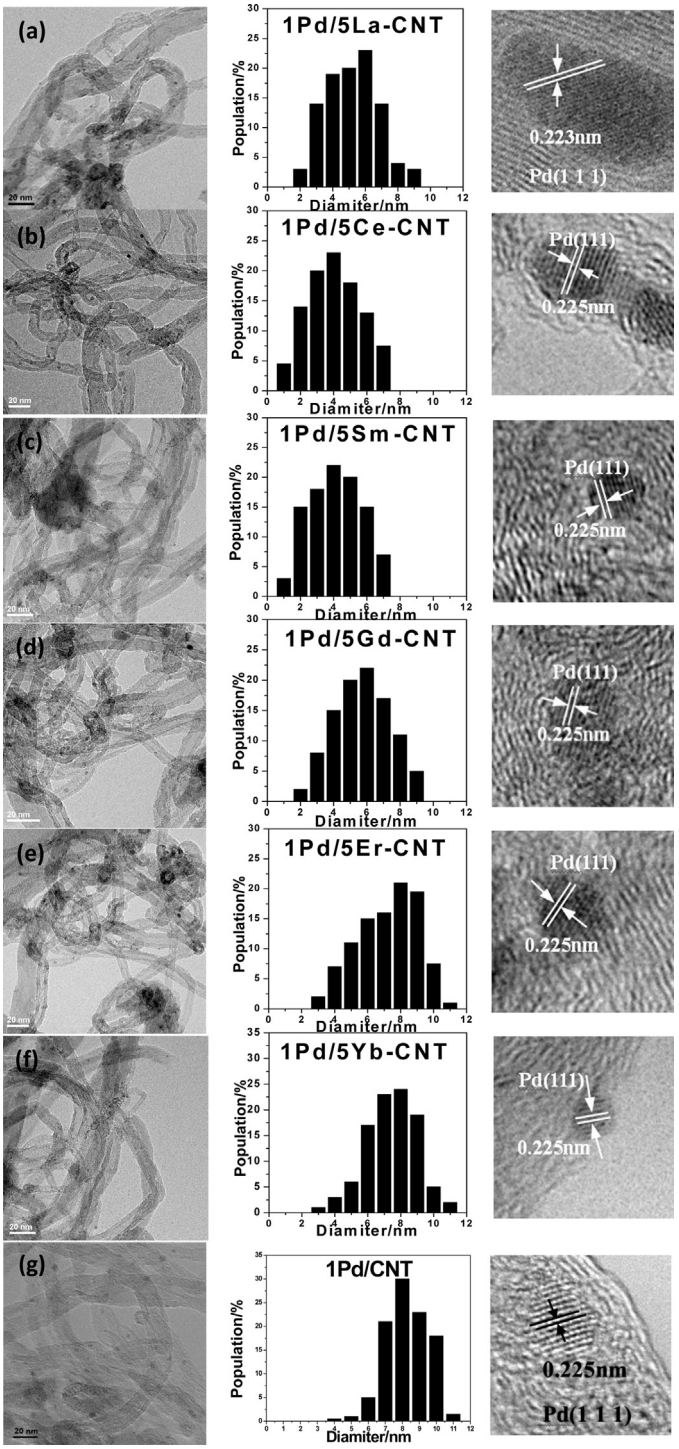

Fig. 2. TEM images and Pd particle size distribution histograms: (a) Pd/5La-CNT; (b) Pd/5Ce-CNT; (c) Pd/5Sm-CNT; (d) Pd/5Gd-CNT; (e) Pd/5Er-CNT; (f) Pd/5Yb-CNT; (g) Pd/CNT.

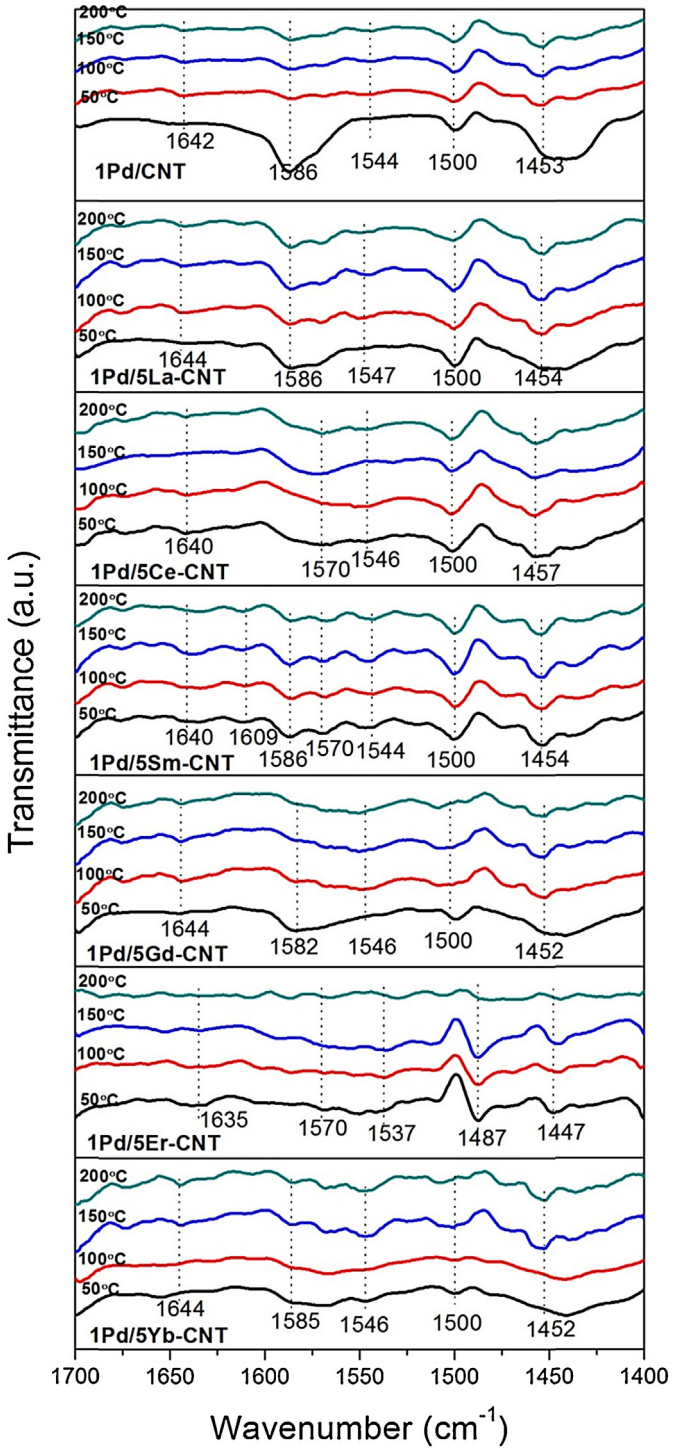

Fig. 3. FTIR spectra of pyridine adsorption on 1Pd/CNT, 1Pd/5La-CNT, 1Pd/5Ce-CNT, 1Pd/5Sm-CNT, 1Pd/5Gd-CNT, 1Pd/5Er-CNT and 1Pd/5Yb-CNT catalysts at different temperatures.

Please cite this article in press as: Y. Yan, et al., Palladium nanoparticles supported on CNT functionalized by rare-earth oxides for solvent-free aerobic oxidation of benzyl alcohol, Catal. Today (2015), http://dx.doi.org/10.1016/j.cattod.2015.07.021

distribution along with an enhanced metal–support interaction, which has been reported by Chen et al. and they suggested that the basicity can significantly impact the catalytic performance in the aerobic oxidation of benzyl alcohol [37]. Furthermore, the electron density is another crucial factor for catalytic performance.

CO stripping voltammetry was performed through electro-oxidation reaction of carbon monoxide. In CO stripping, CO monolayer adsorbed on catalysts will be electro-oxidized to CO_2 at initially a negative voltage and along with the increased sweeping voltage of the working electrode immersed in 1 M of KOH aqueous electrolyte solution. Based on cyclic voltammetry, CO stripping is a practical method to measure the electrochemical active surface (EAS) area of Pd nanoparticles at low Pd loadings [60] because of the low electrical signals ascribed to the release of hydrogen atoms bonded to Pd surfaces as well as the uncertainty caused by the background subtraction [47]. The Langmuir–Hinshelwood mechanism is normally accepted as the model for CO electro-oxidation, where adsorbed OH formed on the Pd surface by dissociative adsorption of H_2O reacts with the adsorbed CO [61].

$$H_2O_{ads} \xrightarrow{k_1} OH_{ads} + H^+ + e^- \quad (1)$$

$$OH_{ads} + H^+ + e^- \xrightarrow{k_2} H_2O_{ads} \quad (2)$$

$$CO_{ads} + OH_{ads} \xrightarrow{k_3} CO_2 + H^+ + e^- \quad (3)$$

The KOH aqueous electrolyte neutralizes the H^+ and pushes the reaction moving forward. Thus CO electro-oxidation potential relies upon the kinetics, thermodynamics and electrochemical state of Pd nanoparticles. Fig. 5 presents the CO stripping voltammograms of 1Pd/CNT and 1Pd/5Ln-CNT catalysts. The negative shifts of onset potentials for CO electro-oxidation indicate the higher catalytic activity for the onset of CO electro-oxidation reaction, suggesting that it is easier to initiate the CO oxidization using rare-earth oxides functionalized 1Pd/5Ln-CNT catalysts. Accordingly, the rare-earth oxides functionalized CNT supported Pd catalysts possess the higher onset catalytic activity than non-functionalized Pd/CNT catalyst, which may due to the improved electron density, electron transition capability and the enhanced metal–support interactions. Among all these catalysts, the 1Pd/5Sm-CNT affords the highest onset catalytic activity for CO oxidation. The EAS areas of Pd particles are calculated with the assumption that the oxidation of CO monolayer adsorbed on surface of 1 cm^2 of Pd nanoparticles requires 420 μC of electric charge [62,63]. The results show that the electrochemical active surface areas are in correspondence with the XRD and TEM measurements (shown in Table 1). Modification with rare-earth oxides, especially Sm_2O_3 and CeO_2, facilitates EAS increase in catalysts due to the smaller particle sizes and the higher dispersion of Pd nanoparticles.

We applied the solvent-free oxidation of benzyl alcohol with molecular oxygen as a model reaction to examine these Pd/CNT and Pd/5Ln-CNT catalysts, in order to elucidate the effect of surface rare-earth oxides functionalities on catalytic performance. The results are listed in Table 1, where qTOF was determined as the number of converted benzyl alcohol molecules per hour over the number of active sites where the number of active sites (i.e., Pd atoms exposed on the particle surface) was determined by EAS value with the Pd content obtained from ICP measurements, subtracting the non-catalytic effect (i.e., ~5% of benzyl alcohol conversion at 160 °C). According to ICP test results in Table 1, the increased Pd contents upon functionalization with rare-earth oxides suggest the enhanced surface hydrophilicity which can reduce the adsorption barrier of palladium aqueous precursor onto the support surfaces. Dehydrogenation of benzyl alcohol already occurs to form benzaldehyde and co-product molecular hydrogen in the absence of O_2. Oxygen is a great hydrogen acceptor to consume H_2 [53]. The main product benzaldehyde is a non-enolizable aldehyde, which limits the number of byproducts. Primary byproducts include toluene from hydrogenolysis of C—O bond of benzyl alcohol where

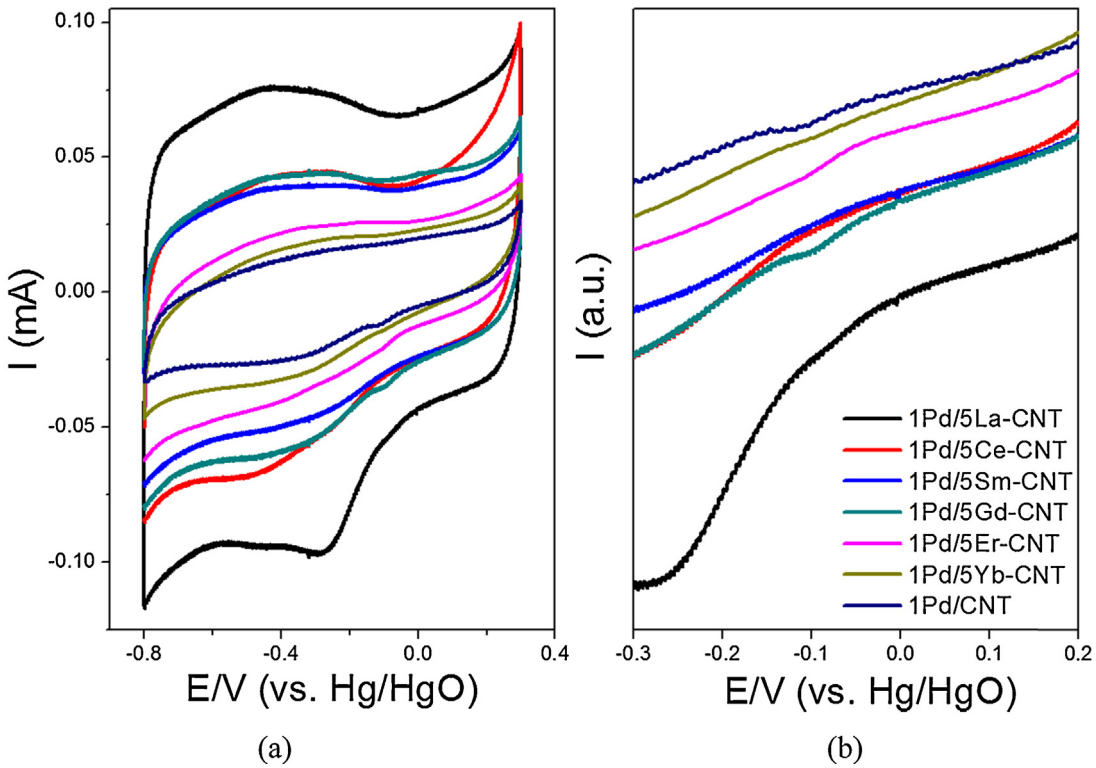

Fig. 4. (a) Cyclic voltammetry curves (CVs) of 1Pd/CNT and 1Pd/5Ln-CNT catalysts in 1 M KOH aqueous solution with a scan rare of 50 mV s^{-1}; (b) magnification of the selected area in (a) presenting Pd-O reduction peaks.

Please cite this article in press as: Y. Yan, et al., Palladium nanoparticles supported on CNT functionalized by rare-earth oxides for solvent-free aerobic oxidation of benzyl alcohol, Catal. Today (2015), http://dx.doi.org/10.1016/j.cattod.2015.07.021

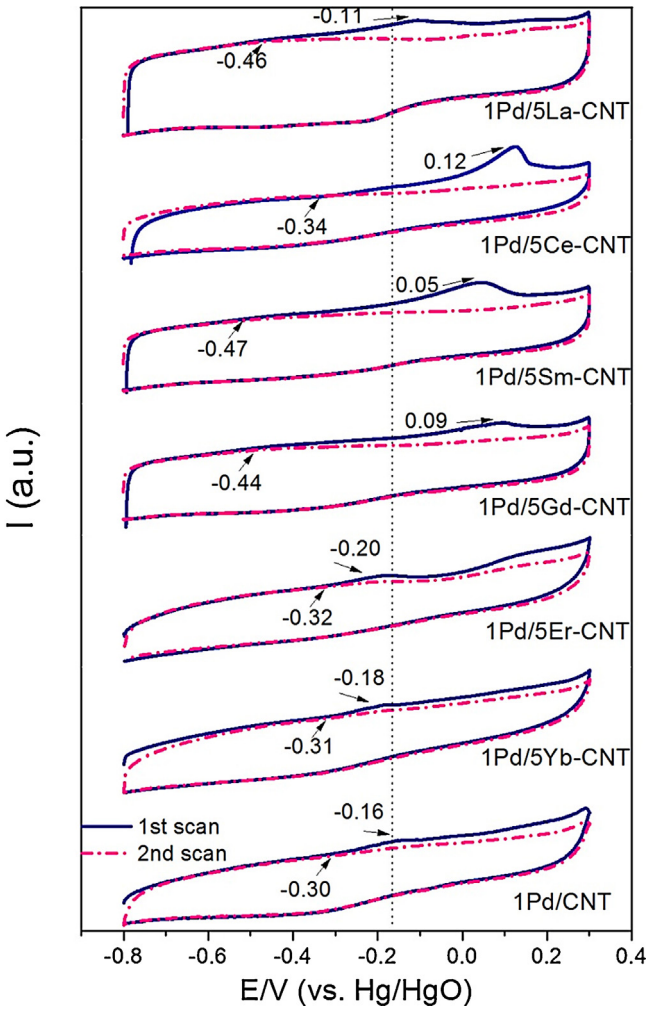

Fig. 5. CO striping voltammograms of 1Pd/5La-CNT, 1Pd/5Ce-CNT, 1Pd/5Sm-CNT, 1Pd/5Gd-CNT, 1Pd/5Er-CNT, 1Pd/5Yb-CNT and 1Pd/CNT catalysts.

hydrogen molecule is formed from dehydrogenation reaction on Pd in reduced state (Pd^0) and benzoic acid formed by hydration of benzaldehyde followed by the dehydrogenation reaction [53].

$$PhCH_2OH \rightarrow PhCHO + H_2 \quad (4)$$

$$PhCH_2OH + H_2 \rightarrow PhCH_3 + H_2O \quad (5)$$

$$PhCHO_{ad} + H_2O_{ad} \rightarrow PhCH(OH)_{2,ad} \quad (6)$$

$$PhCH(OH)_{2,ad} \rightarrow PhCOOH_{ad} + 2H_{ad} \quad (7)$$

In addition, the surface basicity of catalysts favors the disproportionation of benzaldehyde (Cannizzaro reaction), producing benzoic acid and benzyl alcohol [64].

$$2PhCHO + H_2O \xrightarrow{base} PhCH_2O + PhCOOH \quad (8)$$

As shown in Table 1, the catalytic activity is remarkably improved upon the functionalization with rare-earth oxides. Among all the catalysts, 1Pd/5Sm-CNT presents the best catalytic performance with a conversion of 29.6% and an outstanding qTOF of 253,842 h^{-1}, which is 1.5 times higher than that of 1Pd/CNT, owing to the smallest size of Pd nanoparticles [65], improved metal–support interaction, appropriate surface basicity and the abundant thermal stable surface acid sites over 1Pd/5Sm-CNT surfaces. The surface basic site has been reported to cleave the O—H bond to produce alkoxide intermediate while the surface acid site participates in producing and transferring H_2 in dehydrogenation of benzyl alcohol [52], a significant step in its oxidation reaction, since surface acid sites possess better affinity to H_2 [66–68]. Nevertheless, the high activities are accompanied by a large amount of toluene as byproduct, so as to decrease the benzaldehyde selectivity. The formation of toluene further verifies that the Pd is in reduced metallic state (Pd^0) [53], which facilitates the hydrogenolysis of benzyl alcohol when O_2 is not sufficiently supplied or the reaction rate of O_2 consuming H_2 is not rapid enough. The relatively lower selectivity toward toluene over 1Pd/5Sm-CNT than other rare-earth oxides functionalized catalysts is caused by the abundant amount of types of acid sites absorbing the hydrogen from Pd surface on 1Pd/5Sm-CNT, reducing the amount of H_2 on Pd surface. Considering the highest conversion and appropriate selectivity toward benzaldehyde, the Sm_2O_3 was selected as the optimal surface functionality in the following study.

3.2. Effect of Sm_2O_3 amount

CNT functionalized with 2.5 wt.%, 5 wt.%, 7.5 wt.%, 10 wt.% content of Sm in the form of Sm_2O_3 and loaded with 1 wt.% of Pd were prepared for comparison. XRD patterns of samarium oxide functionalized CNT supported Pd catalysts are presented in Fig. 6. The peak width at half height of the peak at 40.00°, related to the characteristic (1 1 1) plane of Pd, increases with the increasing the Sm_2O_3 content, implying the decrease of Pd nanoparticle size according to Scherrer equation, which has been further substantiated by TEM observations shown in Fig. 7. The Pd nanoparticle size decreases in the series of 4.3 nm, 3.7 nm, 3.3 nm and 3 nm, as the Sm_2O_3 content increases in the order of 2.5 wt.%, 5 wt.%, 7.5 wt.% and 10 wt.%. The more amount of Sm_2O_3 functionality facilitates the higher hydrophilicity of CNT surface which favors smaller Pd nanoparticles. Meanwhile, peaks centered at 27.76° and 31.94°, assigned to (1 1 1) and (2 0 0) planes of Sm_2O_3, emerge and intensify as the Sm

Table 1
Catalytic results of benzyl alcohol oxidation over 1Pd/CNT and 1Pd/5Ln-CNT.[a]

Catalyst	Pd content (wt.%)[b]	Ln content (wt.%)[b]	EAS[c] ($m^2\ g^{-1}$)	Conversion (%)	Selectivity (%)			qTOF[d] (h^{-1})
					Benzaldehyde	Toluene	Benzoic Acid	
1Pd/CNT	0.78		12.8	17.2	91.3	7.1	1.6	169,163
1Pd/5La-CNT	0.81	2.81	18.9	26.7	88.6	11.4	0	203,777
1Pd/5Ce-CNT	1.25	1.64	18.4	25.8	85.2	14.4	0.4	201,597
1Pd/5Sm-CNT	0.79	2.06	17.2	29.6	90.4	7.2	2.4	253,842
1Pd/5Gd-CNT	1.08	2.59	14.7	24.5	81.4	18.6	0	235,437
1Pd/5Er-CNT	0.93	2.78	13.9	23.4	84.2	15.8	0	234,942
1Pd/5Yb-CNT	0.91	2.86	13.0	23.0	85.6	13.9	0.5	245,746

[a] Reaction conditions: catalyst, 10 mg (the amount of Pd is 1 wt.% of catalyst, 0.1 mg); benzyl alcohol, 50 mmol; O_2, 20 mL min^{-1}; temperature, 160 °C; time, 1 h.
[b] Real metal content was tested by ICP.
[c] EAS areas were deduced from data of CO stripping.
[d] qTOF is defined as the number of converted benzyl alcohol molecules in 1 h over one active site; the number of active sites (Pd atoms exposed on the surface of particle) is determined by EAS value [63] considering Pd content obtained from ICP, and subtracted the non-catalytic effect (conversion ~5%).

Please cite this article in press as: Y. Yan, et al., Palladium nanoparticles supported on CNT functionalized by rare-earth oxides for solvent-free aerobic oxidation of benzyl alcohol, Catal. Today (2015), http://dx.doi.org/10.1016/j.cattod.2015.07.021

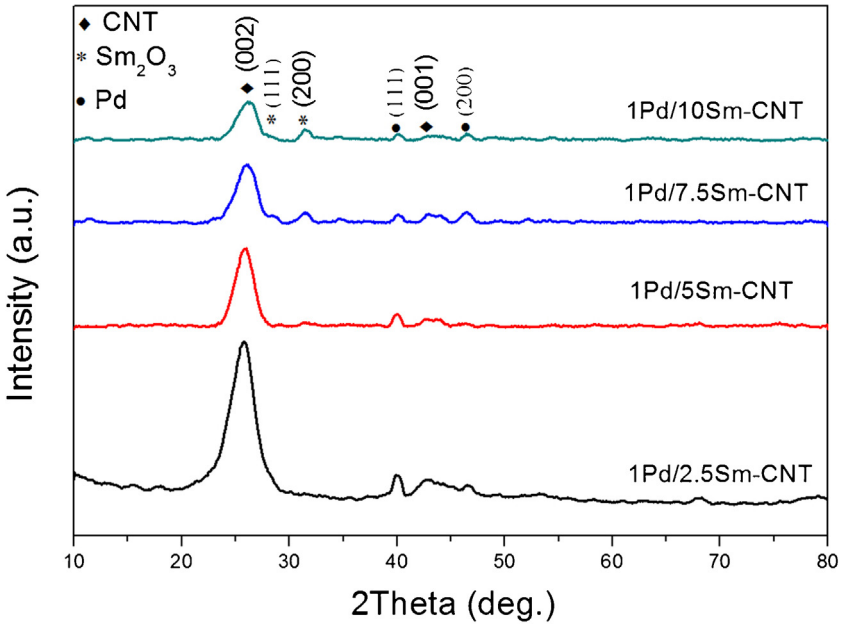

Fig. 6. XRD patterns for 1Pd/Sm_2O_3-CNT with Sm content of 2.5 wt.%, 5 wt.%, 7.5 wt.% and 10 wt.%.

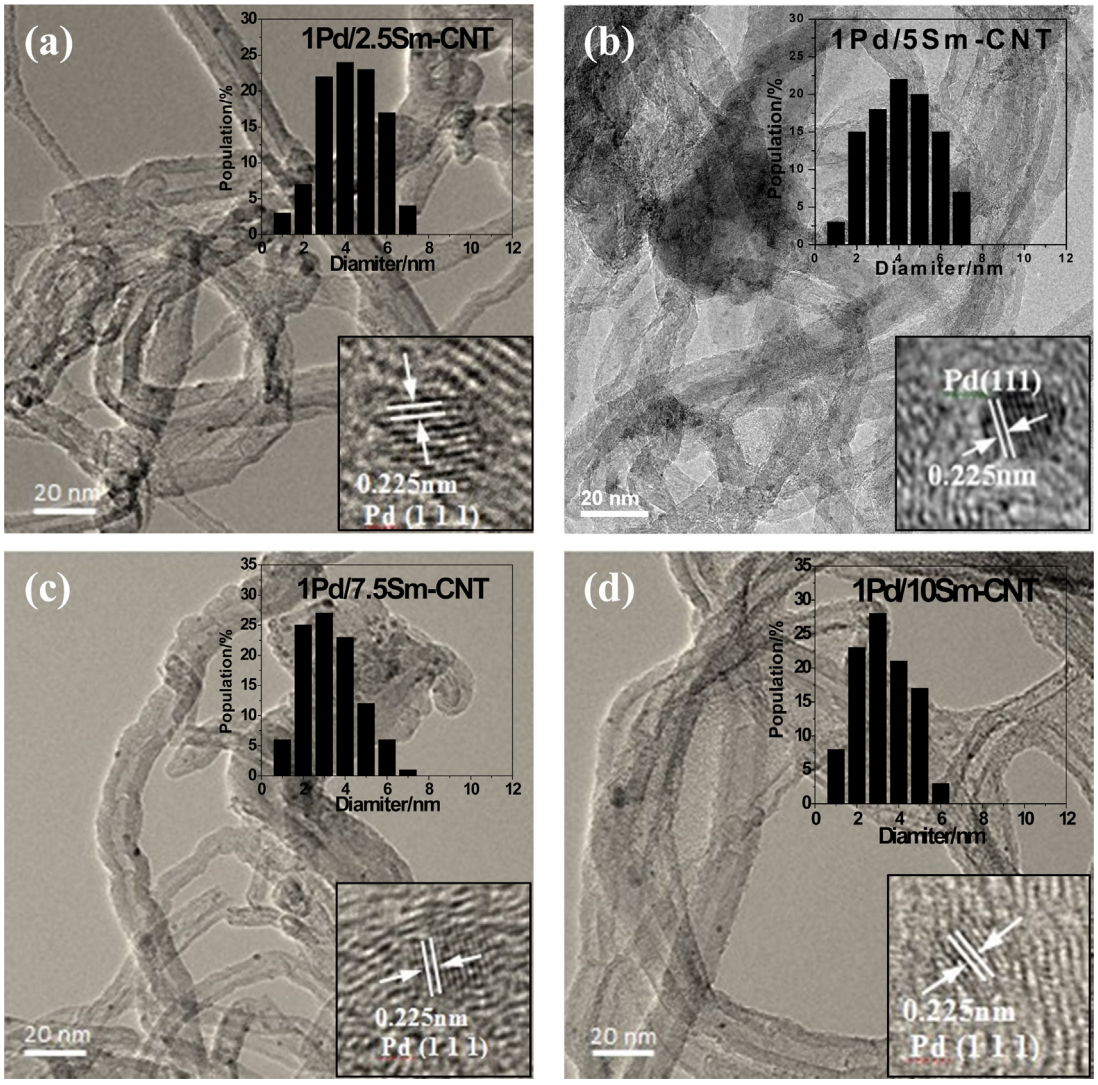

Fig. 7. TEM images and Pd particle size distribution histograms of various amount of Sm_2O_3 functionalized CNT supported Pd catalysts: (a) 1Pd/2.5Sm-CNT; (b) 1Pd/5Sm-CNT; (c) 1Pd/7.5Sm-CNT; (d) 1Pd/10Sm-CNT.

Please cite this article in press as: Y. Yan, et al., Palladium nanoparticles supported on CNT functionalized by rare-earth oxides for solvent-free aerobic oxidation of benzyl alcohol, Catal. Today (2015), http://dx.doi.org/10.1016/j.cattod.2015.07.021

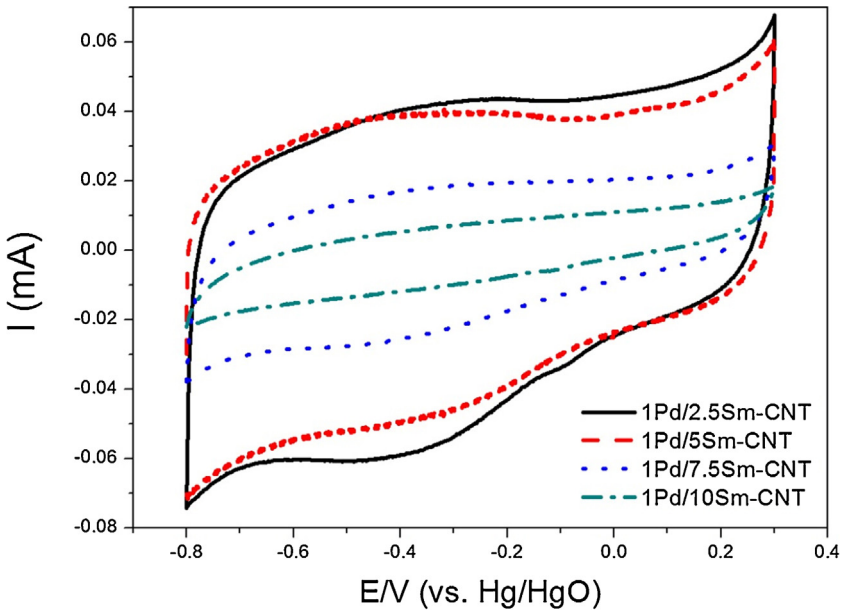

Fig. 8. Cyclic voltammograms (CVs) of 1Pd/2.5Sm-CNT, 1Pd/5Sm-CNT, 1Pd/7.5Sm-CNT and 1Pd/10Sm-CNT catalysts in 1 M KOH electrolyte solution with a scan rate of 50 mV s^{-1}.

content increases from 2.5 wt.% to 10 wt.% in the form of Sm_2O_3, which enables the formation of larger amount of crystal structure of Sm_2O_3.

CV measurements are performed and cyclic voltammograms are shown in Fig. 8. The areas enclosed by CV curves are observed with an evident decrease in the sequence of: 1Pd/2.5Sm-CNT > 1Pd/5Sm-CNT > 1Pd/7.5Sm-CNT > 1Pd/10Sm-CNT. Small content of rare-earth functionalized CNT supported Pd catalyst has larger capacitance and CV background due to the remarkable electron donating properties of Sm_2O_3. Nevertheless, the capacitance and CV background will decline with the further increase of rare-earth oxides content due to the abrupt decrease of the electron conductor (i.e., CNT) content. The redox signal peak of Pd—O bond at ca. −0.09 V is only discernible for 1Pd/2.5Sm-CNT, indicating that the higher content of Sm_2O_3 favors fully reduced Pd (Pd^0) generation and stabilizes the zero-valent status of Pd (Pd^0) nanoparticles.

CO stripping voltammetry was carried out to measure the EAS areas of 1Pd/Sm_2O_3-CNT, as shown in Fig. 9. The EAS area initially increases when Sm content rises from 2.5 wt.% to 5 wt.% and subsequently declines as Sm content rises up to 10 wt.%. The Sm_2O_3 functionalities facilitate the surface hydrophilicity of CNT and hence favor the formation of smaller Pd nanoparticles which possess higher EAS area without the presence of agglomeration at low Sm_2O_3 loadings. Nonetheless, when Sm_2O_3 content gets high enough to form Sm_2O_3 crystalline grains, the metal–support interaction is enhanced with smaller Pd nanoparticles which may reduce the surface exposure of Pd nanoparticles. The mass transfer resistance resulted from the uneven surface after functionalization by large amount of Sm_2O_3 also hampers the contact between Pd and CO molecules and thus results in a smaller EAS area. In addition, higher Sm_2O_3 loadings lead to more direct contact between small Pd nanoparticles and Sm_2O_3 which may reduce the exposure of Pd effective surface to the liquid phase. Among all these samarium oxide functionalized CNT-supported Pd catalysts, 1Pd/5Sm-CNT retains the largest EAS area. Meanwhile, the 1Pd/5Sm-CNT catalyst possesses the lowest onset potential for CO electro-oxidation reaction, indicating its highest onset electrochemical activity for CO electro-oxidation as the model reaction.

Benzyl alcohol oxidation over 1Pd/Sm_2O_3-CNT with different content of Sm_2O_3 was investigated and illustrated in Table 2. Pd

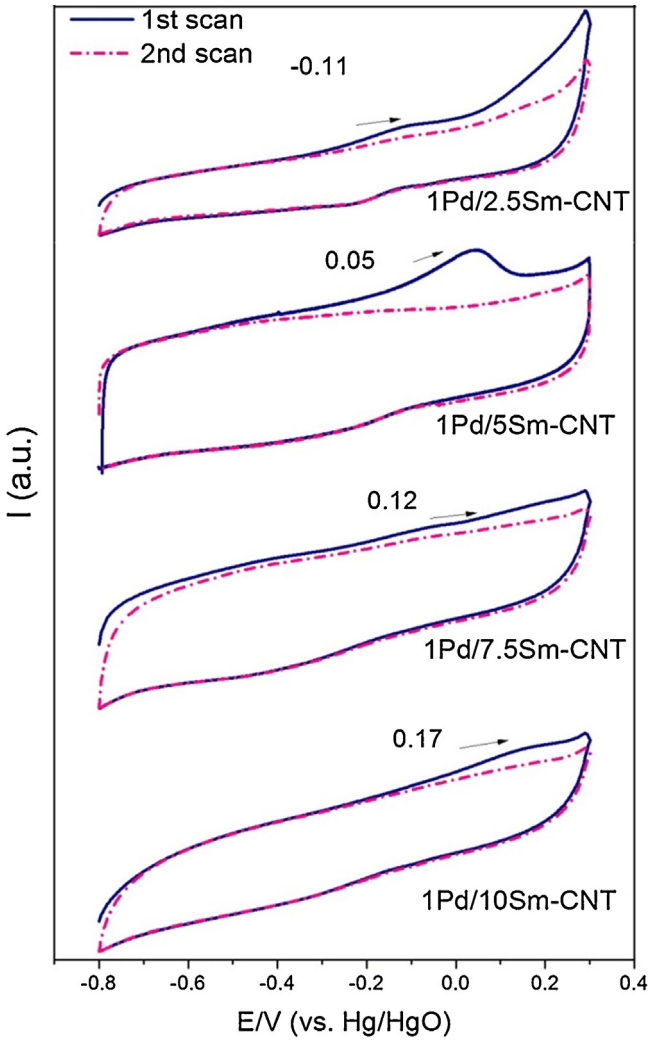

Fig. 9. CO stripping voltammograms of 1Pd/2.5Sm-CNT, 1Pd/5Sm-CNT, 1Pd/7.5Sm-CNT and 1Pd/10Sm-CNT catalysts.

Please cite this article in press as: Y. Yan, et al., Palladium nanoparticles supported on CNT functionalized by rare-earth oxides for solvent-free aerobic oxidation of benzyl alcohol, Catal. Today (2015), http://dx.doi.org/10.1016/j.cattod.2015.07.021

Table 2
Catalytic results of benzyl alcohol oxidation over 1Pd/2.5Sm-CNT, 1Pd/5Sm-CNT, 1Pd/7.5Sm-CNT and 1Pd/10Sm-CNT catalysts.[a]

Catalyst	Pd content (wt.%)[b]	Ln content (wt.%)[b]	EAS[c] ($m^2\ g^{-1}$)	Conversion (%)	Selectivity (%)			qTOF[d] (h^{-1})
					Benzaldehyde	Toluene	Benzoic Acid	
1Pd/CNT	0.78		12.8	17.2	91.3	7.1	1.6	169,163
1Pd/2.5Sm-CNT	0.72	0.66	15.9	28.1	83.3	15.8	0.9	257,853
1Pd/5Sm-CNT	0.79	2.06	17.2	29.6	90.4	7.2	2.4	253,842
1Pd/7.5Sm-CNT	0.83	4.20	11.7	26.1	93.6	4.4	2.0	318,552
1Pd/10Sm-CNT	0.95	6.52	10.3	23.5	95.7	1.5	2.8	318,760

[a] Reaction conditions: catalyst, 10 mg (the amount of Pd is 1 wt.% of catalyst, 0.1 mg); benzyl alcohol, 50 mmol; O_2, 20 mL min^{-1}; temperature, 160 °C; time, 1 h.
[b] Real metal content was tested by ICP.
[c] EAS areas were deduced from data of CO stripping.
[d] qTOF is defined as the number of converted benzyl alcohol molecules in 1 h over one active site; the number of active sites (Pd atoms exposed on the surface of particle) is determined by EAS value [63] considering Pd content obtained from ICP, and subtracted the non-catalytic effect (conversion ~5%).

loading of each catalyst was determined through ICP measurement. The catalytic activity is improved when Sm_2O_3 is doped on CNT surface due to the decreased Pd particle size and synergistic effect from metal–support and metal–functionalities interactions. 1Pd/5Sm-CNT catalyst possesses the highest benzyl alcohol conversion value of 29.6%. Further increasing the Sm_2O_3 loading elevates the qTOF value and selectivity toward benzaldehyde at the sacrifice of EAS area along with the lower conversion value of the substrate benzyl alcohol. The explanation for decrease in EAS area has been illustrated that large amount of Sm_2O_3 functionality enhances the metal–support interaction and the contact area between Pd, Sm_2O_3 and CNT. Both of them decline the exposure of Pd effective area, leading to lower conversion of benzyl alcohol. The trend of qTOF value implies the activity of supported Pd catalysts is primarily dependent on the electrochemical active surface, electron density and surface chemistry surrounding the active phase. Small amount of Sm_2O_3 facilitates the formation of toluene and hence the selectivity toward benzaldehyde is low (83.3%). As the Sm_2O_3 content increases, the selectivity toward benzaldehyde is improved, indicating that the functionalization with an appropriate amount of Sm_2O_3 reduces the formation of byproducts. On account of the highest yield toward the main product benzaldehyde, 1Pd/5Sm-CNT is considered as the optimal catalyst in this study.

3.3. Studies of 1Pd/5Sm-CNT catalyst

The XPS spectra of Pd 3*d* and O 1*s* have been investigated as shown in Fig. 10. The Pd 3*d* peaks were convoluted to Pd^0 and Pd^{2+} two states. The ratios of $Pd^0/(Pd^0+Pd^{2+})$ in Pd/CNT and Pd/5Sm-CNT are 42.3% and 69.7% respectively, indicating the electron donor property of Sm_2O_3 in consistent with the CV results which subsequently enhances the Pd electron density. The shift of $3d_{3/2}$ and $3d_{5/2}$ binding energy peaks of Pd^{2+} toward reduced forms after surface-functionalization with Sm_2O_3 illustrates the lower oxidation extent of Pd or the formation of Pd-Sm_2O_3 complex [69]. The fractions of C—O/C=O of Pd/CNT and Pd/5Sm-CNT are quite close.

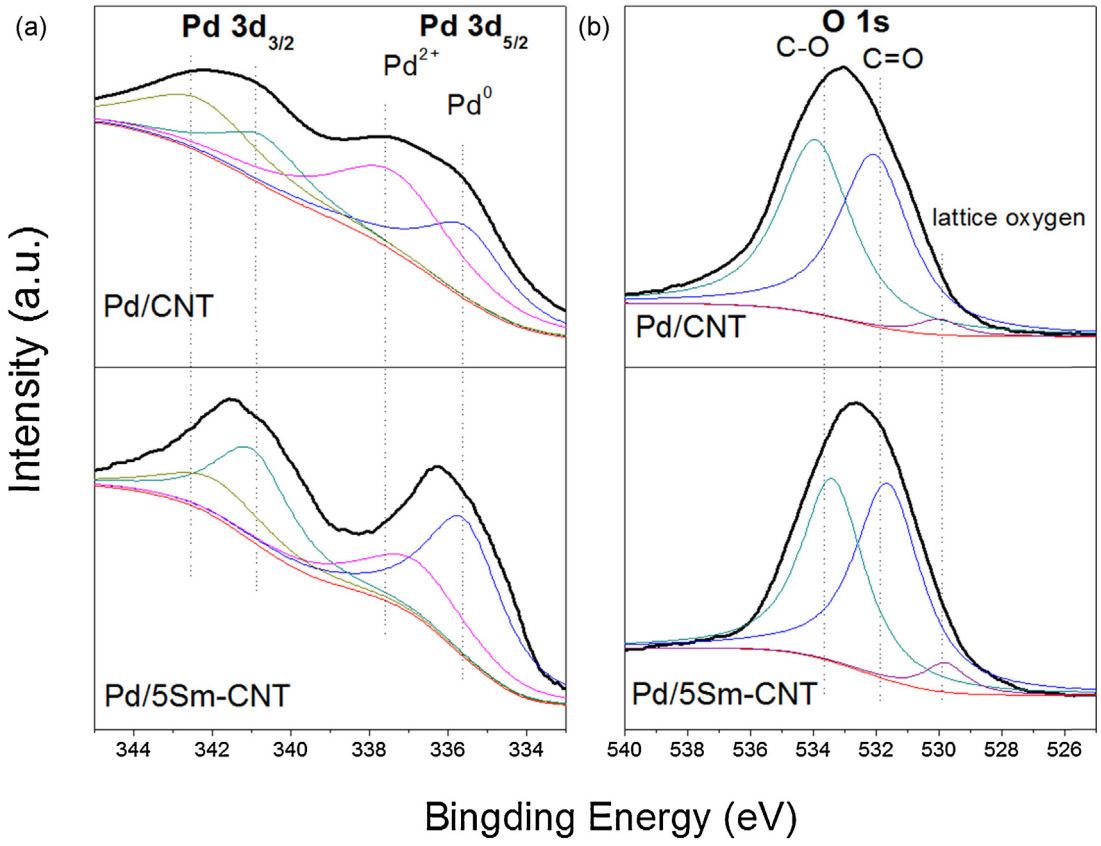

Fig. 10. XPS spectra: (a) Pd 3*d* spectra; (b) O 1*s* spectra of Pd/CNT and Pd/5Sm-CNT.

Please cite this article in press as: Y. Yan, et al., Palladium nanoparticles supported on CNT functionalized by rare-earth oxides for solvent-free aerobic oxidation of benzyl alcohol, Catal. Today (2015), http://dx.doi.org/10.1016/j.cattod.2015.07.021

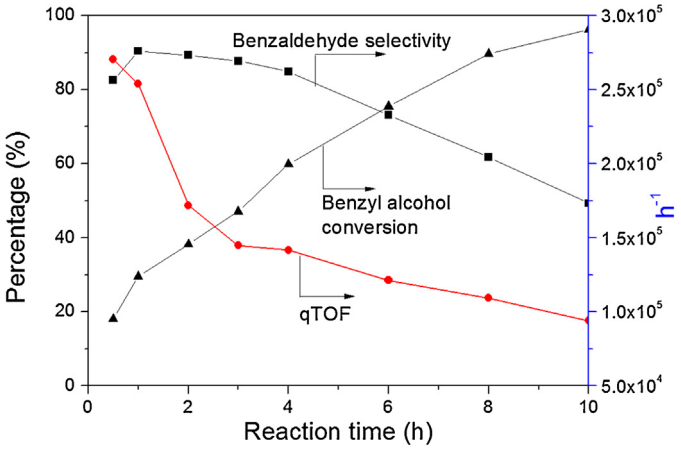

Fig. 11. Time course of 1Pd/5Sm-CNT catalyst for aerobic oxidation of benzyl alcohol (benzyl alcohol/Pd = 500 mol/g; O_2 flow rate, 20 mL min^{-1}; temperature, 160 °C; stirring rate, 1200 rpm).

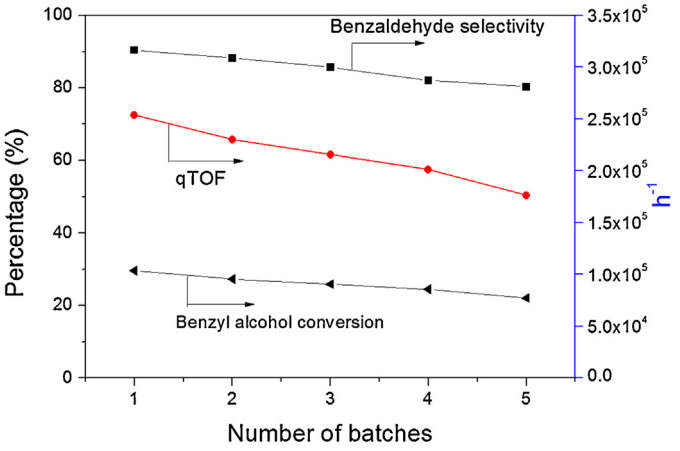

Fig. 12. Recyclability of 1Pd/5Sm-CNT catalyst for solvent-free aerobic oxidation of benzyl alcohol (benzyl alcohol/Pd = 500 mol/g; oxygen flow rate, 20 mL min^{-1}; reaction temperature, 160 °C; time, 1 h; stirring speed, 1200 rpm).

Nonetheless the apparent increase in lattice oxygen of Pd/5Sm-CNT compared to Pd/CNT is explained by the presence of lattice oxygen in Sm_2O_3 surface functionality.

Investigations on 1Pd/5Sm-CNT, which is selected as the best catalyst in solvent-free oxidation of benzyl alcohol, were carried out in detail. Time course of 1Pd/5Sm-CNT in target reaction was detected periodically as shown in Fig. 11. The conversion of benzyl alcohol monotonically increases with the passage of reaction time followed by a monotone decrease of the qTOF value. During the reaction time course, more and more substrate is converted, while due to the decrease of the concentration of substrate, the reaction rate becomes slower which is reflected as the decline in qTOF value. The selectivity toward benzaldehyde is 82.5% at the first 0.5 h. This low selectivity is caused by the high selectivity toward toluene from hydrogenolysis reaction of the C—O bond in benzyl alcohol with the residual H_2 absorbed on Pd from the dehydrogenation reaction. This is in consistence with the mechanism reported by Keresszegi et al. that the dehydrogenation reaction of benzyl alcohol initially exists whether at the absence of molecular oxygen or not [53]. The coproduct H_2 from dehydrogenation reaction is subsequently consumed (1) in the hydrogenolysis of benzyl alcohol to from toluene; and (2) in the oxidation reaction by O_2, which are two parallel competitive reactions. Evidently, O_2 is a much superior hydrogen acceptor than benzyl alcohol, consuming almost all the H_2 and suppressing the extent of hydrogenolysis reaction [30]. With the reaction time going on, more benzaldehyde is formed and partially further oxidized to benzoic acid, which explains the decrease of selectivity toward benzaldehyde after 1 h.

The recyclability is regarded as a vital factor in the evaluation of heterogeneous catalyst in a multiphase reaction. The active phase with poor stability and reusability may leach out during the reaction, and the metallic components producing susceptible by-products in a reaction might get poisoned, bringing about the loss of catalytic activity for subsequent runs of target reaction. The recyclability of 1Pd/5Sm-CNT in the solvent-free aerobic oxidation of benzyl alcohol using gaseous oxygen has been investigated, as displayed in Fig. 12. The catalyst was manually recovered after each reaction batch by washing with acetone, drying at 60 °C and recharged in the next reaction batch. The operation was repeated four times and 1Pd/5Sm-CNT was used in five consecutive runs. The conversion, selectivity and qTOF are accompanied by a moderate decrease, which is ascribed to the loss of active surface area of metallic phase. The Pd content after the five consecutive cycles remains almost the same as the as-prepared catalyst. The Pd content is not detectable by ICP analysis in the filtrate phase after any batch of reaction, indicating that no leaching of Pd occurs during reactions and the immobilization of metal phase on support has been stabilized after the surface-functionalization of Sm_2O_3. Therefore, the samarium oxide surface-functionalized CNT supported Pd catalysts possess not merely the improved catalytic performance in benzyl alcohol oxidation, but also the superiority in the resistance against deactivation.

4. Conclusions

In this work, Pd nanoparticle catalysts supported on rare-earth oxide functionalized CNT surfaces Pd/LnO_x-CNT (Ln = La, Ce, Sm, Gd, Er, Yb) have been prepared using wet impregnation method followed with a metal ion adsorption–reduction process. Rare-earth oxides functionalities presented great influence on the catalytic performances. The XRD, TEM, HRTEM, ICP, pyridine adsorption FTIR, and electrochemical measurements such as CV and CO stripping analysis suggested the impact of rare-earth oxides functionalities on Pd nanoparticle size, Pd valence, electron densities, EAS areas, chemistry environment of active phase and synergistic effect from metal–support interactions, along with the impact on catalytic performance for solvent-free selective aerobic oxidation of benzyl alcohol. Sm_2O_3 surface functionalized CNT with an appropriate amount of Sm_2O_3 loading exhibited the best improvement. Among all the catalysts, 1Pd/5Sm-CNT possessed the highest conversion value of 29.6% whereas 1Pd/10Sm-CNT had the highest qTOF value of 318,760 h^{-1} and selectivity of 95.7% toward benzaldehyde.

Acknowledgements

We acknowledge the financial support from the National Research Foundation (NRF), Prime Minister's Office, Singapore under its Campus for Research Excellence and Technological Enterprise (CREATE) program and AcRF Tier 1 grant (RG129/14), Ministry of Education, Singapore.

References

[1] L. Vivier, D. Duprez, ChemSusChem 3 (2010) 654–678.
[2] A.G. Dedov, A.S. Loktev, I.I. Moiseev, A. Aboukais, J.F. Lamonier, I.N. Filimonov, Appl. Catal. A: Gen. 245 (2003) 209–220.
[3] S. Arndt, J. Okuda, Adv. Synth. Catal. 347 (2005) 339–354.
[4] Y. Luo, M. Nishiura, Z. Hou, J. Organomet. Chem. 692 (2007) 536–544.
[5] G. Sun, X. Mu, Y. Zhang, Y. Cui, G. Xia, Z. Chen, Catal. Commun. 12 (2011) 349–352.
[6] M. Ozawa, Y. Nishio, J. Alloys Compd. 374 (2004) 397–400.

Please cite this article in press as: Y. Yan, et al., Palladium nanoparticles supported on CNT functionalized by rare-earth oxides for solvent-free aerobic oxidation of benzyl alcohol, Catal. Today (2015), http://dx.doi.org/10.1016/j.cattod.2015.07.021

[7] M. Ozawa, J. Alloys Compd. 408–412 (2006) 1090–1095.
[8] O.V. Mokhnachuk, S.O. Soloviev, A.Y. Kapran, Catal. Today 119 (2007) 145–151.
[9] S. Valange, A. Beauchaud, J. Barrault, Z. Gabelica, M. Daturi, F. Can, J. Catal. 251 (2007) 113–122.
[10] R. Liu, C. Zhang, J. Ma, J. Rare Earths 28 (2010) 376–382.
[11] L. Hensgen, K. Stowe, Catal. Today 159 (2011) 100–107.
[12] M. Sugiura, Catal. Surv. Asia 7 (2003) 77–87.
[13] K. Krishna, A. Bueno-López, M. Makkee, J.A. Moulijn, Top. Catal. 42–43 (2007) 221–228.
[14] R.C. Martins, N. Amaral-Silva, R.M. Quinta-Ferreira, Appl. Catal. B: Environ. 99 (2010) 135–144.
[15] Y.F. Ying, Y.J. Wang, M.F. Luo, J. Rare Earths 25 (2007) 249–252.
[16] F. Wang, G.X. Lu, J. Power Sources 181 (2008) 120–126.
[17] S.E.J. Hackett, R.M. Brydson, M.H. Gass, I. Harvey, A.D. Newman, K. Wilson, A.F. Lee, Angew. Chem. Int. Ed. 46 (2007) 8593–8596.
[18] A.H. Lu, W.C. Li, Z.S. Hou, F. Schuth, Chem. Commun. (2007) 1038–1040.
[19] S.H. Liu, R.F. Lu, S.J. Huang, A.Y. Lo, S.H. Chien, S.B. Liu, Chem. Commun. (2006) 3435–3437.
[20] Y. Yan, J. Miao, Z. Yang, F.-X. Xiao, H.B. Yang, B. Liu, Y. Yang, Chem. Soc. Rev. 44 (2015) 3295–3346.
[21] P. Serp, E. Castillejos, ChemCatChem 2 (2010) 41–47.
[22] K.P. De Jong, J.W. Geus, Catal. Rev. 42 (2000) 481–510.
[23] P. Serp, M. Corrias, P. Kalck, Appl. Catal. A: Gen. 253 (2003) 337–358.
[24] C. Zhou, H. Wang, F. Peng, J. Liang, H. Yu, J. Yang, Langmuir 25 (2009) 7711–7717.
[25] M.W. Wang, F.Y. Li, N.C. Peng, 新型炭材料 17 (2002) 75–79.
[26] T. Fujigaya, N. Nakashima, Adv. Mater. 25 (2013) 1666–1681.
[27] J. Pritchard, L. Kesavan, M. Piccinini, Q. He, R. Tiruvalam, N. Dimitratos, J.A. Lopez-Sanchez, A.F. Carley, J.K. Edwards, C.J. Kiely, G.J. Hutchings, Langmuir 26 (2010) 16568–16577.
[28] S. Meenakshisundaram, E. Nowicka, P.J. Miedziak, G.L. Brett, R.L. Jenkins, N. Dimitratos, S.H. Taylor, D.W. Knight, D. Bethell, G.J. Hutchings, Faraday Dis. 145 (2010) 341–356.
[29] N. Dimitratos, J.A. Lopez-Sanchez, D. Morgan, A.F. Carley, R. Tiruvalam, C.J. Kiely, D. Bethell, G.J. Hutchings, Phys. Chem. Chem. Phys. 11 (2009) 5142–5153.
[30] Y.B. Yan, Y.T. Chen, X.L. Jia, Y.H. Yang, Appl. Catal. B: Environ. 156 (2014) 385–397.
[31] R. Arrigo, S. Wrabetz, M.E. Schuster, D. Wang, A. Villa, D. Rosenthal, F. Girsgdies, G. Weinberg, L. Prati, R. Schloegl, D.S. Su, Phys. Chem. Chem. Phys. 14 (2012) 10523–10532.
[32] H.T. Tan, Y.T. Chen, C.M. Zhou, X.L. Jia, J.X. Zhu, J. Chen, X.H. Rui, Q.Y. Yan, Y.H. Yang, Appl. Catal. B: Environ. 119 (2012) 166–174.
[33] T. Harada, S. Ikeda, M. Miyazaki, T. Sakata, H. Mori, M. Matsumura, J. Mol. Catal. A: Chem. 268 (2007) 59–64.
[34] A. Villa, D. Wang, N. Dimitratos, D. Su, V. Trevisan, L. Prati, Catal. Today 150 (2010) 8–15.
[35] Y.-S. Chi, H.-P. Lin, C.-Y. Mou, Appl. Catal. A: Gen. 284 (2005) 199–206.
[36] H. Sun, Q.H. Tang, Y. Du, X.B. Liu, Y. Chen, Y.H. Yang, J. Colloid Interface Sci. 333 (2009) 317–323.
[37] Y.T. Chen, Z. Guo, T. Chen, Y.H. Yang, J. Catal. 275 (2010) 11–24.
[38] S. Wu, Q. He, C. Zhou, X. Qi, X. Huang, Z. Yin, Y. Yang, H. Zhang, Nanoscale 4 (2012) 2478–2483.
[39] F. Wolfers, C. R. Hebd. Des Seances Acad. Des Sci. 177 (1923) 759–762.
[40] H.G. Jiang, M. Ruhle, E.J. Lavernia, J. Mater. Res. 14 (1999) 549–559.
[41] A.L. Patterson, Phys. Rev. 56 (1939) 978–982.
[42] T. Blasco, A. Galli, J.M.L. Nieto, F. Trifiro, J. Catal. 169 (1997) 203–211.
[43] Q. Sun, Y.C. Fu, J. Liu, A. Auroux, J.Y. Shen, Appl. Catal. A: Gen. 334 (2008) 26–34.
[44] J. Keranen, A. Auroux, S. Ek, L. Niinisto, Appl. Catal. A: Gen. 228 (2002) 213–225.
[45] S.Q. Hu, D.P. Liu, L.S. Li, Z. Guo, Y.T. Chen, A. Borgna, Y.H. Yang, Chem. Eng. J. 165 (2010) 916–923.
[46] T. Mathew, B.B. Tope, N.R. Shiju, S.G. Hegde, B.S. Rao, C.S. Gopinath, Phys. Chem. Chem. Phys. 4 (2002) 4260–4267.
[47] Z. Guo, Y.T. Chen, L.S. Li, X.M. Wang, G.L. Haller, Y.H. Yang, J. Catal. 276 (2010) 314–326.
[48] A. Gervasini, A. Auroux, J. Catal. 131 (1991) 190–198.
[49] M. Ai, T. Ikawa, J. Catal. 40 (1975) 203–211.
[50] M. Ai, J. Catal. 40 (1975) 318–326.
[51] M. Ai, J. Catal. 40 (1975) 327–333.
[52] W. Fang, J. Chen, Q. Zhang, W. Deng, Y. Wang, Chem. – Eur. J. 17 (2011) 1247–1256.
[53] C. Keresszegi, D. Ferri, T. Mallat, A. Baiker, J. Phys. Chem. B 109 (2005) 958–967.
[54] S. Sugunan, G. Devikarani, J. Mater. Sci. Lett. 10 (1991) 887–888.
[55] S. Sugunan, G.D. Rani, K.B. Sherly, React. Kinet. Catal. Lett. 43 (1991) 375–380.
[56] S. Sugunan, K.B. Sherly, G.D. Rani, React. Kinet. Catal. Lett. 51 (1993) 525–532.
[57] S. Sugunan, G.D. Rani, Indian J. Chem. Sect. A: Inorg. Phys. Theor. Anal. Chem. 32 (1993) 993–995.
[58] N.S. Lawrence, R.P. Deo, J. Wang, Electroanalysis 17 (2005) 65–72.
[59] S. Sato, R. Takahashi, M. Kobune, H. Gotoh, Appl. Catal. A: Gen. 356 (2009) 57–63.
[60] K. Jukk, N. Alexeyeva, C. Johans, K. Kontturi, K. Tammeveski, J. Electroanal. Chem. 666 (2012) 67–75.
[61] C. Saravanan, N.M. Markovic, M. Head-Gordon, P.N. Ross, J. Chem. Phys. 114 (2001) 6404–6412.
[62] L.L. Fang, Q.A. Tao, M.F. Li, L.W. Liao, D. Chen, Y.X. Chen, Chin. J. Chem. Phys. 23 (2010) 543–548.
[63] S.X. Wu, Q.Y. He, C.M. Zhou, X.Y. Qi, X. Huang, Z.Y. Yin, Y.H. Yang, H. Zhang, Nanoscale 4 (2012) 2478–2483.
[64] C.G. Swain, A.L. Powell, W.A. Sheppard, C.R. Morgan, J. Am. Chem. Soc. 101 (1979) 3576–3583.
[65] F. Li, Q.H. Zhang, Y. Wang, Appl. Catal. A: Gen. 334 (2008) 217–226.
[66] S. Ramachandran, J.H. Ha, D.K. Kim, Catal. Commun. 8 (2007) 1934–1938.
[67] R.K. Agarwal, J.S. Noh, J.A. Schwarz, P. Davini, Carbon 25 (1987) 219–226.
[68] J.S. Noh, R.K. Agarwal, J.A. Schwarz, Int. J. Hydrogen Energy 12 (1987) 693–700.
[69] A. Gniewek, A.M. Trzeciak, J.J. Ziółkowski, L. Kępiński, J. Wrzyszcz, W. Tylus, J. Catal. 229 (2005) 332–343.

Please cite this article in press as: Y. Yan, et al., Palladium nanoparticles supported on CNT functionalized by rare-earth oxides for solvent-free aerobic oxidation of benzyl alcohol, Catal. Today (2015), http://dx.doi.org/10.1016/j.cattod.2015.07.021